Numerical treatment of state-dependent permeability in multiphysics problems

Ivar Stefansson[1], **Eirik Keilegavlen**[1]

[1]Center for Modeling of Coupled Subsurface Dynamics, Department of Mathematics, University of Bergen

Key Points:

- State-dependent permeability produces strong nonlinearity in multiphysics problems
- Ignoring state dependency in solution scheme severely impacts convergence
- A novel approach differentiating the finite volume flux stencil greatly improves nonlinear convergence

Corresponding author: Eirik Keilegavlen, Eirik.Keilegavlen@uib.no

Abstract

Constitutive laws relating fluid potentials and fluxes in a nonlinear manner are common in several porous media applications, including biological and reactive flows, poromechanics, and fracture deformation. Compared to the standard, linear Darcy's law, such enhanced flux relations increase both the degree of nonlinearity, and, in the case of multiphysics simulations, coupling strength between processes. While incorporating the nonlinearities into simulation models is thus paramount for computational efficiency, correct linearization, as is needed for incorporation in Newton's method, is challenging from a practical perspective. The standard approach is therefore to ignore nonlinearities in the permeability during linearization. For finite volume methods, which are popular in porous media applications, complete linearization is feasible only for the simplest flux discretization, namely the two-point flux approximation. We introduce an approximated linearization scheme for finite volume methods that is exact for the two-point scheme and can be applied to more advanced and accurate discretizations, exemplified herein by a multi-point flux stencil. We test the new method for both nonlinear porous media flow and several multiphysics simulations. Our results show that the new linearization consistently outperforms the standard approach. Moreover our scheme achieves asymptotic second order convergence of the Newton iterations, in contrast to the linear convergence obtained with the standard approach.

1 Introduction

The topic of this paper is porous media simulation models where the fluid flux is related to pressure through a nonlinear diffusion law. We will refer to constitutive laws that have permeability as a dynamic function of other variables as state-dependent permeability relations. They are important in several porous media applications, including well-established models such as Richards' equation in hydrology (Richards, 1931) and the cubic relation between fracture aperture and permeability (Boussinesq, 1868). Other constitutive relations of relevance to this work are power laws and the Kozeny-Carman relation between porosity and permeability (Hommel et al., 2018), and bulk permeability as a function of the effective pressure (Shapiro, 2015). These examples illustrate that constitutive permeability relations appear in both single-physics models that are essentially of nonlinear diffusion type and complex multiphysics problems where the permeability in modeled as functionally dependent on several primary variables.

In numerical simulations, the cost of linearization, and of solving the resulting linear problem, will typically dominate the overall cost of simulation, thus the solution strategy for nonlinear terms is critical for simulation efficiency. Common approaches for solving nonlinear systems can be divided into three classes: The simplest approach is the straightforward application of Newton's method, which achieves second order convergence rate in the asymptotic limit, but is only locally convergent (Deuflhard, 2005). Methods in the second class attempt to achieve global convergence by combining Newton's method with schemes such as line searches (Dennis Jr & Schnabel, 1996), trust region approaches (Jenny et al., 2009; Wang & Tchelepi, 2013; Møyner, 2017), fixed-point methods (Radu et al., 2015), and acceleration methods (Anderson, 1965; Walker & Ni, 2011; Jiang & Tchelepi, 2019). Some of these techniques can be applied at the start of a nonlinear solve when the approximated solution is presumed to be outside the Newton convergence region, but then apply Newton's method to achieve second order convergence for the last iterations, e.g., (List & Radu, 2016; Both et al., 2019). Finally, in multiphysics problems, the problem may be split into smaller blocks that each represent one or several physical processes, and Newton's method applied successively to each of these blocks (Jenny et al., 2006; Li et al., 2021).

Independent of which of the above strategies is applied, it is highly desirable that the linearization scheme is implemented so that second order accuracy can be achieved

asymptotically. This depends on the Jacobian containing sufficiently accurate (ideally exact) representations of the multivariate derivatives of the residual equations. Depending on the design of the simulation software, correctly implementing the derivatives involves tedious work, and including new nonlinearities, for instance in the form of permeability relations, can be a tremendous technical challenge. While these technicalities can be partly relieved by employing automatic differentiation to construct the derivatives, as is increasingly being done in simulation software (Krogstad et al., 2015; Zhou et al., 2011; Rasmussen et al., 2021), a simpler alternative is to ignore or approximate derivatives in the linearization scheme. The resulting scheme can be considered a quasi-Newton approach, in the sense that the Jacobian matrix is not the true derivative of the residual equations. Relying on such approximated Jacobian matrices can significantly simplify implementation, thus adaptation, of new physical models, but as with any quasi-Newton method, second order convergence can in general not be achieved (Nocedal & Wright, 1999). A critical question in employing Newton's method in multiphysics simulations, in particular when considering non-standard effects such as nonlinear permeability relations, is therefore whether the derivatives can be computed with sufficient accuracy to preserve second order convergence, and whether the speedup gained is worth the additional implementation effort.

Since linearization is applied to the discretized system, the question of how to calculate or approximate derivatives is closely linked to the discretization methods in use. Specifically, for state-dependent permeability relations, the discretization of diffusion terms must be differentiated with respect to the relevant primary variables. This can readily be done for methods based on variational formulations, including primal and mixed finite elements. However, in finite volume methods, which are commonly applied for complex applications, the permeability enters the discretization in non-trivial ways, and exact derivatives can be obtained only in some cases. Specifically, it is relatively straightforward to differentiate the two-point flux approximation (TPFA) (Aziz & Settari, 1979) with respect to permeability. While robust, this scheme is well known to suffer from inconsistencies and grid orientation effects, see e.g. (Zhou et al., 2011). More advanced finite volume methods, in this paper exemplified by the so-called multi-point flux approximation (MPFA) methods (Aavatsmark, 2002; Edwards & Rodgers, 1998), amend these shortcomings. However, the more complex discretization stencils in such methods are not readily differentiated, raising the question of whether fast Newton convergence can be achieved when the discretizations are applied to (multiphysics) problems with state-dependent permeability relations. As an alternative, some versions of nonlinear finite volume methods, e.g. (Su et al., 2018), can be applied within Newton's method. However, few applications of nonlinear methods to multiphysics problems have been reported, see (Schneider et al., 2018) for an exception, and we are not aware of any application of nonlinear finite volume methods to problems with state-dependent permeability.

In the present work, we study multiphysics problems involving state-dependent permeability. We restrict ourselves to fully coupled solution strategies based on implicit temporal discretization and finite volume approximations of spatial derivatives. We thus disregard approaches based on decoupling or tailoring of the nonlinear solver, however, the techniques we introduce can also be applied to such approaches. We consider both TPFA and MPFA methods. For the more complex MPFA scheme it is not practical to calculate exact derivatives, and we therefore show how to approximate the derivatives by a TPFA approach. Our suggested method is easy to implement and can readily be applied to multiphysics problems. We illustrate this by presenting simulations of four problems of high application relevance: A nonlinear diffusive flow problem, a reactive transport problem where permeability is altered by chemical dissolution, poromechanical simulations where the permeability changes due to porosity changes, and hydro-mechanical simulations for fractured porous media, with the fracture permeability changing due to fracture deformation. In all cases, we show that our formulation is superior to the standard treatment of permeability updates, leading to much reduced simulation time. All sim-

ulations are run using PorePy, an open-source simulation toolbox for multiphysics problems in fractured porous media (Keilegavlen et al., 2021), see Section 6.

The rest of the paper is structured as follows: Section 2 presents the model equations for fluid flow and the three multiphysics example models. In Section 3, we describe the finite volume flux discretizations and our proposed method for including permeability updates. Section 4 contains results for validation and application simulations, while we offer a summary and conclusions in Section 5.

2 Example model problems

In this section we introduce four model problems that motivate our study of solvers that deal with state-dependent permeability. These are a nonlinear stationary diffusion problem and three multiphysics problems which each illustrate different mechanisms leading to dynamic and nonlinear permeability, which in turn impact the entire nonlinear system of equations. We use the four problems to validate and illustrate our discretization scheme in Section 4.

For all applications, we model the fluid flux q using nonlinear version of Darcy's law:

$$q = -\mathbb{K}(\xi)\nabla p, \tag{1}$$

with p representing the potential. Throughout this work we will use the fluid pressure as the potential, and we will assume a constant fluid viscosity of 1. The permeability $\mathbb{K}$ depends on the system state, represented here by a generic variable ξ. For single physics nonlinear diffusion $\xi = p$, while for the multiphysics problems considered in the following sections more advanced dependencies will be introduced. In the case $\xi = p$, a state-dependent diffusion problem can be obtained by combining Eq. (1) with a conservation equation, which reads:

$$\frac{\partial \phi \rho}{\partial t} + \nabla \cdot (\rho q) = f. \tag{2}$$

Here, ϕ is a porosity, t the time variable and f a fluid source term. The fluid density is

$$\rho = \rho_0 e^{c(p-p_0)}, \tag{3}$$

with c and ρ_0 denoting compressibility and reference density, respectively. For simplicity, we shall sometimes consider an incompressible fluid, i.e., $c = 0$. Setting $c = 0$ in (2) gives a nonlinear stationary diffusion model.

2.1 Reactive transport

As our first multiphysics application we consider reactive transport with mineral dissolution. We represent this by a kinetic reaction system of two components, denoted A and B, represented by the pore volume fractions c_A and c_B, where A is aqueous and B is a mineral. Conservation of the two components is modeled as

$$\frac{\partial \phi c_A \rho_A}{\partial t} + \nabla \cdot (q c_A \rho_A) = r \tag{4}$$

$$\frac{\partial c_B \rho_B}{\partial t} = -r \tag{5}$$

Here, the reaction term is $r = r_0\Big(c_A/K_A - 1\Big)$ with r_0 denoting a constant reference reaction rate, the Darcy velocity q is computed using Eq. (1) and K_A denotes the concentration at which component A is in equilibrium. The component densities are represented by ρ_A and ρ_B, and are taken as constant in this work. For simplicity, we assume the fluid density function is independent of c_A so that water conservation is described by (2).

The porosity will change with the concentration of the mineral B, i.e.

$$\phi = \phi_0(1 - c_B), \tag{6}$$

where ϕ_0 is the reference porosity at $c_B = 0$. The permeability will also be altered by the reactions, commonly modeled by the power law

$$\mathbb{K} = \mathbb{K}_0 \Big(\frac{\phi}{\phi_0}\Big)^{\eta}, \tag{7}$$

with $\mathbb{K}_0$ denoting the permeability at the reference porosity and the exponent η an application dependent fitting parameter (Hommel et al., 2018). The presence of q in Eq. (4) and the permeability's porosity dependence result in a two-way coupled problem.

2.2 Poroelasticity

A common model for coupled flow and mechanical deformation in a porous medium is described by the equations which read (Coussy, 2004)

$$\begin{aligned} \nabla \cdot (\mathbb{C}\epsilon - I\alpha p) &= f_s & (8)\\ \frac{\partial \rho\phi}{\partial t} - \nabla \cdot (\rho \mathbb{K} \nabla p) &= f_f & (9) \end{aligned}$$

Here, $\epsilon = (\nabla u + (\nabla u)^T)/2$ is the symmetric strain tensor, u is the displacement vector, and the Darcy velocity q is explicitly represented in the equations for illustrative purposes. Furthermore, $\mathbb{C}$ represents the stiffness matrix, I the identity tensor, α is the Biot coefficient, f_m is body forces, and f_s denotes fluid source terms. The porosity depends on both fluid pressure and the displacement (Coussy, 2004)

$$\phi = \phi_0 + (1 - \alpha)\frac{\alpha - \phi_0}{K_s}(p - p_0) + \alpha \nabla \cdot (u - u_0), \tag{10}$$

with K_s denoting the bulk modulus and where ϕ_0, p_0, and u_0 represent porosity, pressure, and displacement in a reference state. The permeability will change together with the porosity, modeled herein by setting $\eta = 3$ in Eq. (7), resulting in the Kozeny-Carman relation. The Biot coefficient α thus acts as a control on the direct contribution from the mechanical deformation to the (nonlinear) permeability change.

2.3 Fractured poroelastic medium with dynamic fracture aperture

As a final example application, we consider the extension of poroelasticity to fractured media. Several models exist for deformation of fractured media, we consider a simple version which nevertheless illustrates the importance of dynamic permeability effects in the fracture, through the dependency of fracture aperture.

We consider a domain with a single fracture, which is modeled as a lower-dimensional inclusion embedded in the simulation domain; extensions to networks of intersecting fractures is straightforward, see for instance (Stefansson et al., 2021). Flow and deformation of the host medium are again modeled as a poroelastic system, i.e., by Eqs. (8) - (10). Fluid flow in the fracture and between fracture and matrix are modeled by Darcy-type laws on the form (Martin et al., 2005; Nordbotten et al., 2019)

$$q_{\parallel} = -\mathbb{K}_{\parallel} \nabla_{\parallel} p_f, \qquad q_{\perp}^{\pm} = \kappa_{\perp}(p_{\perp}^{\pm} - p_f), \tag{11}$$

In these equations, subscripts $\parallel$ and $\perp$ represent the tangential and normal direction to the fracture, respectively, while superscript $\pm$ indicates the two sides of the fracture; we

refer to (Nordbotten et al., 2019) for more details. The fracture permeability is related to the fracture aperture a through the so-called cubic law,

$$K_{\|} = \frac{a^3}{12}. \tag{12}$$

Mass conservation for the host medium is modeled by (2), while in the fracture, the equation reads

$$\frac{\partial(\rho a)}{\partial t} + \nabla \cdot (\rho q_{\|}) - \rho(q_{\perp}^{+} + q_{\perp}^{-}) = f \tag{13}$$

where the last term of the left-hand side describes inflow into fracture from the host domain.

The aperture can change due to mechanical deformation of the fracture. A wide range of models have been proposed to incorporate such effects under various circumstances, see e.g. (Barton et al., 1985; Willis-Richards et al., 1996). As a simple but illustrative example, consider the effective traction T on the fracture wall,

$$T = n \cdot (\mathbb{C}\epsilon - I p_m) - p_f I \cdot n. \tag{14}$$

When the normal component of the effective traction is tensile, the fracture walls are pushed apart, leading to an increasing aperture

$$a = [u]_n + a_0 \qquad [u] = u^{+} - u^{-}, \tag{15}$$

where $u^{\pm}$ is the displacement on the opposing fracture walls, subscript n denotes the normal component and a_0 is a residual hydraulic aperture. Changes in the aperture are coupled through the fracture permeability to the pressure equation in the fracture, with coupling of the fracture pressure back to the effective normal traction as shown by the last term of Eq. (14).

In the normal direction to the fracture, its deformation is restricted by

$$[u]_n \geq 0 \qquad [u]_n T_n = 0 \qquad T_n \leq 0. \tag{16}$$

Denoting the friction coefficient by F, we model the tangential (τ) deformation using a Coulomb type friction law, see e.g.,(Hüeber & Wohlmuth, 2005):

$$||T_\tau|| \leq -F T_n \tag{17}$$

$$||T_\tau|| < -F T_n \Rightarrow [u]_\tau = 0 \tag{18}$$

$$||T_\tau|| = -F T_n \Rightarrow \exists\, \zeta \in \mathbb{R}^{+} : [u]_\tau = \zeta T_\tau. \tag{19}$$

These equations are supplemented by a condition of force balance on the fracture walls, i.e.,

$$T^{+} + T^{-} = 0 \tag{20}$$

where again superscripts are used to denote quantities on the two opposing sides of the fracture.

3 Discretization

In this section, we briefly introduce two finite volume methods for diffusive terms. Then, we show how to extend them for state-dependent permeability.

3.1 Finite Volume Methods

Consider a grid and let Γ_j denote a generic face in the grid. A cell-centered finite volume discretization approximates the flux through Γ_j as

$$q_j = \sum_{i \in \mathcal{T}_j} t_{j,i} p_i, \tag{21}$$

where $\mathcal{T}_j$ represents a set of cells in the vicinity of face j, p_i is the pressure in cell i and the coefficients $t_{j,i}$ are called transmissibilities. The choice of a specific discretization method fixes $\mathcal{T}_j$ and determines how the transmissibilities are computed. As an example, in TPFA, $\mathcal{T}_j$ contains the two immediate neighbors of face j, denoted L and R, and

$$t_{j,L} = \frac{\alpha_L \alpha_R}{\alpha_L + \alpha_R}, \qquad \alpha_i = |\Gamma_j| \frac{n_j \cdot \mathbb{K}_i}{d_{j,i} \cdot d_{j,i}} \cdot d_{j,i}, \qquad t_{j,R} = -t_{j,L}. \tag{22}$$

Here, $i \in L, R$, n_j is the normal vector of Γ_j pointing from cell L to R and $d_{j,L}$ is the distance between the centers of cell L and Γ_j etc. We have defined a positive flux going from cell L to R and $\alpha_{\{L,R\}}$ are known as the half transmissibilities.

In MPFA methods $\mathcal{T}_j$ is larger, for the standard MPFA-O method (specifically the MPFA O(0)-method, see (Aavatsmark, 2002)) it consists of all cells sharing at least one vertex with Γ_j. This makes the construction of the transmissibilities more involved, specifically the construction requires the inversion of a local matrix as detailed in e.g. (Aavatsmark, 2002; Edwards & Rodgers, 1998), and it is therefore not practical to express the transmissibilities explicitly as functions of the permeability.

Equipped with a flux discretization on the form (21) for all faces in a grid, the integral form of the flux divergence in (2), stated for a cell ω_k with boundary $\partial\omega_k$ and outer normal vector n, reads

$$\int_{\partial\omega_k} q \cdot n \, dS \approx \sum_{j \in \mathcal{F}_k} q_j = \sum_{j \in \mathcal{F}_k} \sum_{i \in \mathcal{T}_j} t_{j,i} p_i, \tag{23}$$

with $\mathcal{F}_k$ denoting the set of faces of ω_k.

3.2 Discrete state-dependent permeability

The discretization defined by Eq. (21) is routinely applied both to stand-alone diffusion problems and multiphysics problems that include diffusion as part of larger problems, both linear and nonlinear. In cases where the permeability depends on the state variable ξ, we have

$$t = t\left(\mathbb{K}\left(\xi\right)\right). \tag{24}$$

For clarity of presentation, we let $\mathbb{K}$ be a scalar so that differentiation is well defined. The below reasoning can be extended to anisotropic and full permeability tensors by differentiating with respect to individual tensor components, which is straightforward but tedious. When applying Newton's method to nonlinear problems that include Eq. (21), we need the differential, which reads

$$dq_j = \sum_{i \in \mathcal{T}_j} \left(t_{j,i} dp_i + \frac{\partial t_{j,i}}{\partial \mathbb{K}_i} \frac{\partial \mathbb{K}_i}{\partial \xi} d\xi \right). \tag{25}$$

While the first term is standard, the second term represents the dependency of the transmissibilities on the cell-wise permeability $\mathbb{K}_i$, which in turn is a function of ξ. For most finite volume discretizations, a direct relation between transmissibility and permeability is not available, thus computing $\frac{\partial t_{j,i}}{\partial \mathbb{K}}$ is not a practical option. The simpler option is therefore to ignore the second term in Newton linearization schemes and rather use an approximated Jacobian. As discussed in the introduction and demonstrated in Section 4, this approximation can reduce the performance of the nonlinear solver, substantially increasing the computational cost of simulations.

From Eq. (22), we see that for TPFA, the term $\frac{\partial t_{j,i}}{\partial \mathbb{K}}$ can be expressed in closed form using the chain rule. If the diffusion term is discretized with TPFA and the second term of Eq. (25) is included, the resulting Jacobian matrix is exact. For other schemes (represented herein by the MPFA method), including a TPFA-based representation of the

second term of Eq. (25) will only give an approximation of the true derivative of the discretized flux. Nevertheless, the approximated scheme will contain information of how diffusion changes with permeability. Thus, compared to the standard approach of ignoring the effect of permeability changes on the Newton search direction, there is reason to hope that the new approach will result in overall lower computational cost, also for other finite volume methods than TPFA.

3.3 Discretization of remaining terms

For the simulations presented in Section 4, the reminder of the terms in the governing equations are discretized by well-estabilshed methods; for completeness, we give a brief summary of the approaches below. The primary variable of the discrete fluxes discussed above is cell-center pressure in the porous matrix. In the case involving fractures, we also have cell pressures in the lower-dimensional grid representing the fracture and fracture-matrix interface fluxes representing $q_{\perp}^{\pm}$ of Eq. (11). The fracture application also requires discrete fracture tractions and interface displacements, as well as matrix displacements which are also used in mono-dimensional poroelasticity. For more information, we refer to (Stefansson et al., 2021). In the reactive transport application, C_A and C_B are also represented by cell-center values. The governing equations are all solved fully coupled using a Newton-Raphson method, with suitable adjustment in the case of contact mechanics as outlined below.

All volume terms are discretized in the standard finite volume manner, i.e. treated as cell-wise constant and integrated over the cell yielding a cell volume factor. The advective terms are discretized using first-order upstream weighting. The upstream direction is computed from the fluid fluxes at the previous nonlinear iteration, while the flux magnitudes are treated fully implicitly. We discretize the poroelastic system with the finite volume multi-point stress approximation scheme (Nordbotten, 2016; Keilegavlen & Nordbotten, 2017), which can be considered a vector extension of the MPFA scheme.

The fracture contact mechanics relations of Eqs. (16) and (17) are reformulated as two complementary functions depending on cell-wise fracture contact traction and fracture wall displacements (Hüeber & Wohlmuth, 2005):

$$C_n = -T_n - \frac{1}{F}\max(0, b_f) \tag{26}$$

and

$$C_\tau = \max(||T_\tau + \tilde{c}[\dot{u}]_\tau||(-T_\tau) + \max(0, b_f(T_\tau + \tilde{c}[\dot{u}]_\tau)). \tag{27}$$

Here $b_f = -F(T_n + \tilde{c}[u]_n)$ is the friction bound, $\dot{u}$ indicates the increment of u between successive time steps and c denotes a numerical constant. The constraints are imposed by setting $C = 0$ and including the two sets of equations in the global equation system, solved using a semi-smooth Newton-Raphson algorithm (Hüeber & Wohlmuth, 2005; Berge et al., 2020) assembled using PorePy's automatic differentiation capability. The resulting linear systems are solved with a direct banded solver (Bollhöfer et al., 2020).

4 Results

In this section, we compare the proposed method to that of standard finite volume schemes in terms of the convergence properties of the nonlinear system. We include the two-point and multi-point method with and without transmissibility differentiation, yielding four combinations which we will refer to as TPD, MPD, TP and MP, respectively. We reiterate that TPD and MPD both apply a TPFA-based approximation of the second term in Eq. (25), the methods only differ in how the transmissibilities in the first term is computed.

All simulations use the open-source software framework PorePy (Keilegavlen et al., 2021), and the simulations can be reproduced in a Docker container that can be found at (Stefansson & Keilegavlen, 2023).

4.1 Fluid flow

First, we perform tests for a range of spatial meshes, thus demonstrating robustness with respect to factors which may impair convergence. Throughout this section, we consider a fluid mass balance problem defined by Eqs. (1) and (2). We consider an incompressible fluid, thus the first term in (2) is dropped, and let the permeability depend on the potential only, i.e. $\xi = p$. Specifically, we consider the function

$$\mathbb{K}(p) = \sqrt{p} + 10^{-2}, \tag{28}$$

with the constant 10^{-2} avoiding negative values due to numerical rounding errors. We consider the manufactured solution $p = x(1-x)y(1-y)$ and apply the resulting source function and homogeneous Dirichlet conditions at the boundary of a unit square domain.

In the first comparison, we use Cartesian meshes with 10, 100 and 500 cells in each dimension and employ the TP and TPD discretizations. We do not include the MP versions, since they reduce to their TP equivalents on Cartesian meshes for isotropic permeability, see (Aavatsmark, 2002). The plots of residual errors in Fig. 4.1 consistently show linear convergence of the reference method and quadratic convergence of the new method. Throughout this section, we use the cell-wise discrete l^2 norm normalized by the square root of the length of the residual vector. Similarly, we compute permeability errors as the l^2 norm of the difference between cell-wise permeability at each iteration and the permeability values in the converged state normalized using the square root of the number of cells. This error is also plotted in Fig. 4.1, demonstrating correlation between the reduction rate of, respectively, the nonlinear residuals and permeability errors.

Next, we apply all four methods to a randomly perturbed structured mesh and an unstructured simplicial mesh, see Fig. 4.1. The discrepancy between TPFA and MPFA means the MPD combination degrades from a full Newton scheme to a Quasi-Newton scheme as discussed in Section 3.2. Thus, quadratic convergence in Newton's method cannot be expected for the latter combination. This is reflected in the difference between results for MPD and TPD in the bottom left convergence plots in Fig. 4.1. Nevertheless, MPD achieves significant improvement over the lagged permeability update in MP. Furthermore, for the TPD combination, quadratic convergence is retained. We note that compromising consistency using TPFA as the base discretization may in certain cases be expedient for its ease of implementation and simulation speed.

Thirdly, we show results for anisotropically distorted meshes considering only MPFA schemes. Fixing the number of cells to 50 in the x direction, we impose grid anisotropy by using 200 and 1000 cells in the y direction before randomly perturbing the nodes (see rightmost close-up in Fig. 2). The perturbation distance is drawn uniformly from $[-dx/4, dx/4]$ and $[-dy/4, dy/4]$, with dx and dy denoting average cell lengths in the two spatial dimensions. Since permeability anisotropy and grid aspect ratio have an indistinguishable effect in TPFA and MPFA methods, see e.g. (Aavatsmark, 2002), this is equivalent to solving a problem with anisotropic permeability. As evident from Fig. 1, convergence deteriorates somewhat with increasing anisotropy, as can be expected since the TPFA-style approximation of the derivatives deviates increasingly from the true MPFA derivatives. Still, significant improvement from the reference method is achieved even for the most extreme anisotropy ratio.

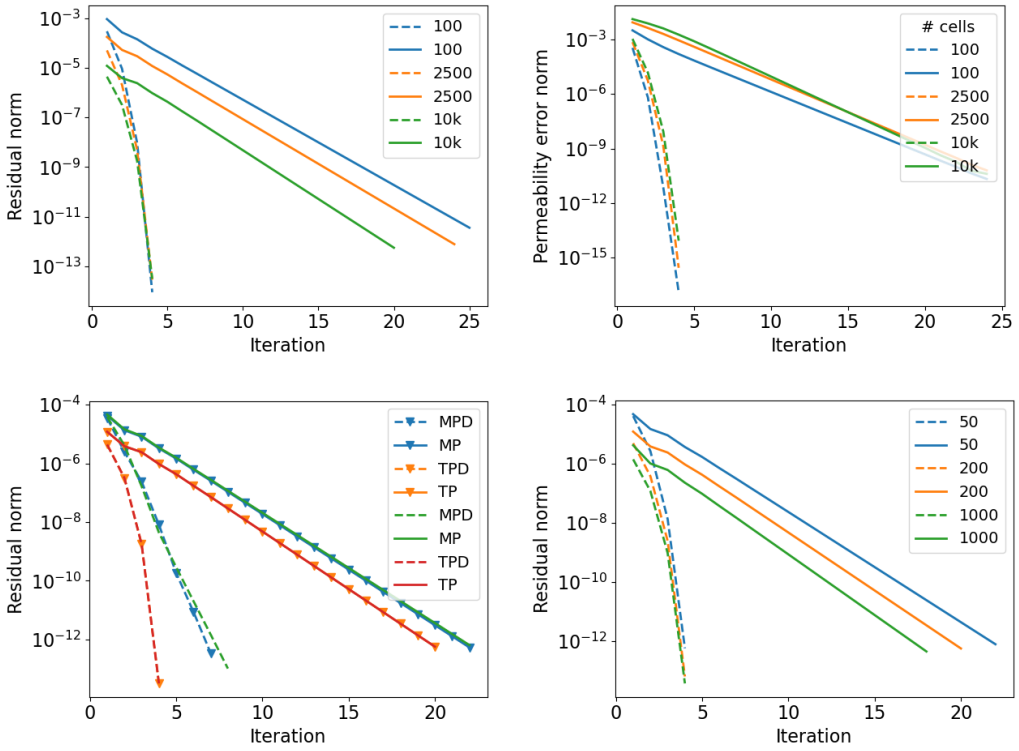

Figure 1. Convergence rates for different cell sizes (top left), different mesh types and discretization schemes (bottom left) and varying degree of mesh anisotropy (bottom right). For the mesh refinement study, the permeability error is also shown (top right). We use solid lines for TP and MP and dashed lines for TPD and MPD. The bottom left plot contains results for tetrahedral and pertubed Cartesian meshes, the former of which are identified with triangular markers.

4.2 Multiphysics applications

We now present three examples of multiphysics applications involving state-dependent permeability. Compared to nonlinear diffusion, the multiphysics models contain additional nonlinearities to the permeability relation, implying that the observed convergence rates are affected by other parts of the solution scheme in addition to the handling of the nonlinear flux. While the models have a wide range of highly relevant applications, the parameters, which are listed in Table 1, are exemplary and do not correspond to particular applications. Having demonstrated robustness with respect to mesh size in the previous section, we apply relatively coarse meshes throughout this section. All grids are Cartesian, meaning that the MPFA and TPFA schemes are equivalent, and we show only results for TP and TPD.

We assign homogeneous Dirichlet boundary conditions for all primary variables, and a source or sink at the domain center acts as the driving force. Initial conditions are zero where not otherwise stated. We use an implicit Euler discretization, consider a single time step and solve the resulting system of equations monolithically.

4.2.1 Reactive transport

Our first application example considers reactive transport as described in Section 2.1. The simulation domain is a unit cube discretized with a Cartesian grid consisting

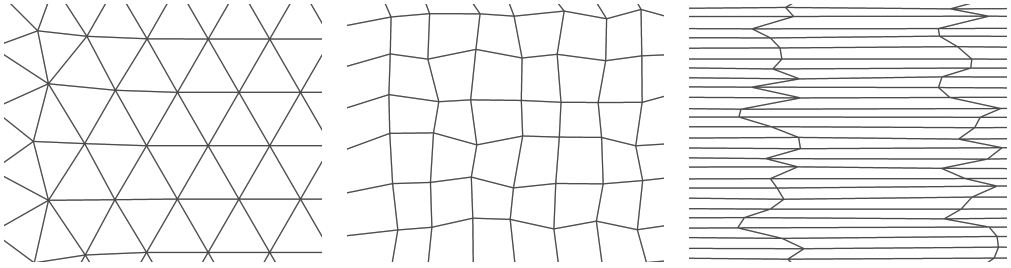

Figure 2. Close-up of a simplex mesh (left) and perturbed meshes with no anisotropy (center) and the anisotropy ratio 50/1000 (right).

Table 1. Parameters used for the application simulations in Sec. 4.2.

Parameter	4.2.1	4.2.2	4.2.3
Reference porosity ϕ_0	5×10^{-2}		
Reference density ρ_0	$1\,\mathrm{kg\,m^{-3}}$		
$\mathbb{K}_0$	$1 \times 10^{-4}\,\mathrm{m^2}$	$1 \times 10^{-5}\,\mathrm{m^2}$	
$\rho_A = \rho_B$	$1\,\mathrm{kg\,m^{-3}}$	-	-
Compressibility c	$0\,\mathrm{Pa^{-1}}$	$1 \times 10^{-3}\,\mathrm{Pa^{-1}}$	$1 \times 10^{-3}\,\mathrm{Pa^{-1}}$
Reaction rate r_0	$4 \times 10^{-1}\,\mathrm{s^{-1}}$	-	-
Equilibrium constant K_A	2×10^{-1}	-	-
Simulation time & time step	$1\,\mathrm{s}$	$1 \times 10^{5}\,\mathrm{s}$	$1 \times 10^{5}\,\mathrm{s}$
Biot coefficient α	-	0.25 to 1	0.2
Lamé parameters μ and λ	-	$1 \times 10^{3}\,\mathrm{Pa}$ and $1 \times 10^{3}\,\mathrm{Pa}$	
Gap g	-	-	$1 \times 10^{-2}\,\mathrm{m}$
Friction coefficient F	-	-	1
Residual aperture a_0	-	-	$1 \times 10^{-1}\,\mathrm{m}$
Numerical constant $\tilde{c}$	-	-	1
Fluid source	$-1 \times 10^{3}\,\mathrm{kg\,s^{-1}}$	$10\,\mathrm{kg\,s^{-1}}$	$10\,\mathrm{kg\,s^{-1}}$ to $40\,\mathrm{kg\,s^{-1}}$

of $15^3 = 3375$ 3d cells. We assign a sink term in the cell at the center of the domain, resulting in flow from the boundary to the center. The initial state is in equilibrium, with $C_A = 0.2$, $C_B = 0.2$ and $p = 0\,\mathrm{Pa}$ matching the Dirichlet boundary pressure. The boundary solute concentration equals 0.4 (twice the initial concentration) causing precipitation. The precipitation in turn reduces porosity and thereby permeability according to Eqs. (6) and (7). The changes to concentration, volume fraction, porosity and permeability are illustrated in Fig. 3.

We consider a series of simulations varying the exponent η of the porosity-permeability relationship in Eq. (7), with the higher values corresponding to a stronger nonlinearity. The range of values explored are identified as relevant for precipitation and dissolution processes, see Bernabe et al. (Bernabé et al., 2003). We provide solution plots in Fig. 3. These show that the dynamics are mainly localized close to the domain boundary, as may be expected in a problem dominated by advection.

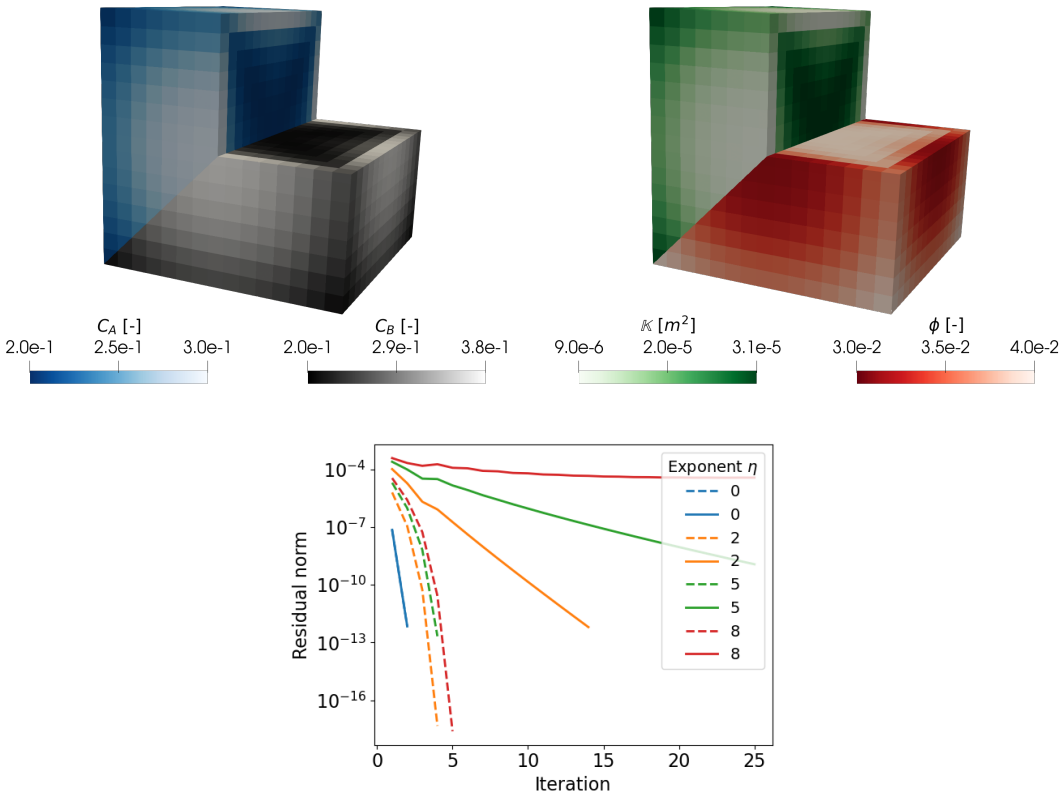

Figure 3. Solution plots for η=5 (top) and convergence rates (bottom) for the reactive transport simulation. We show solute concentration (C_A) and precipitate volume fraction (C_B) to the left and permeability ($\mathbb{K}$) and porosity changes (ϕ) to the right. The simulation domain has been sliced to expose the solution in the interior and different quantities are shown for each half of the slice using separate color maps.

Figure 3 also contains convergence rates demonstrating considerable improvement and asymptotically quadratic behavior for the TPD scheme. In the case $\eta = 0$, the permeability is constant, and the two schemes are equivalent, as evident from the coinciding residual plots. For nonzero values of the exponent η the residual produced by TPD are consistently lower than that of the non-differentiated scheme. The TP residuals deviate considerably in later iterations and the residual reduction is only linear. For the highest value $\eta = 8$, convergence is lost altogether.

4.2.2 Poroelasticity

In poroelasticity, porosity changes caused by pressure and deformation translate into permeability changes, as described in Section 2.2. We again consider the unit cube, with the same spatial grid as in Section 4.2.1 and with a source in the middle of the domain. Fluid injection elevates the pressure and thereby induces displacement in the vicinity of the injection point as shown at the top left in Fig. 4 The displacement in turn influences the permeability through Eqs. (7) and (10). The effect is illustrated in Fig. 5. In our simulation series, we vary the Biot coefficient α in the interval $[0.25, 1]$.

Convergence rates for the Newton schemes are summarized in Fig. 4, showing how the linear model convergence rate decreases with increasing α. The TPD version con-

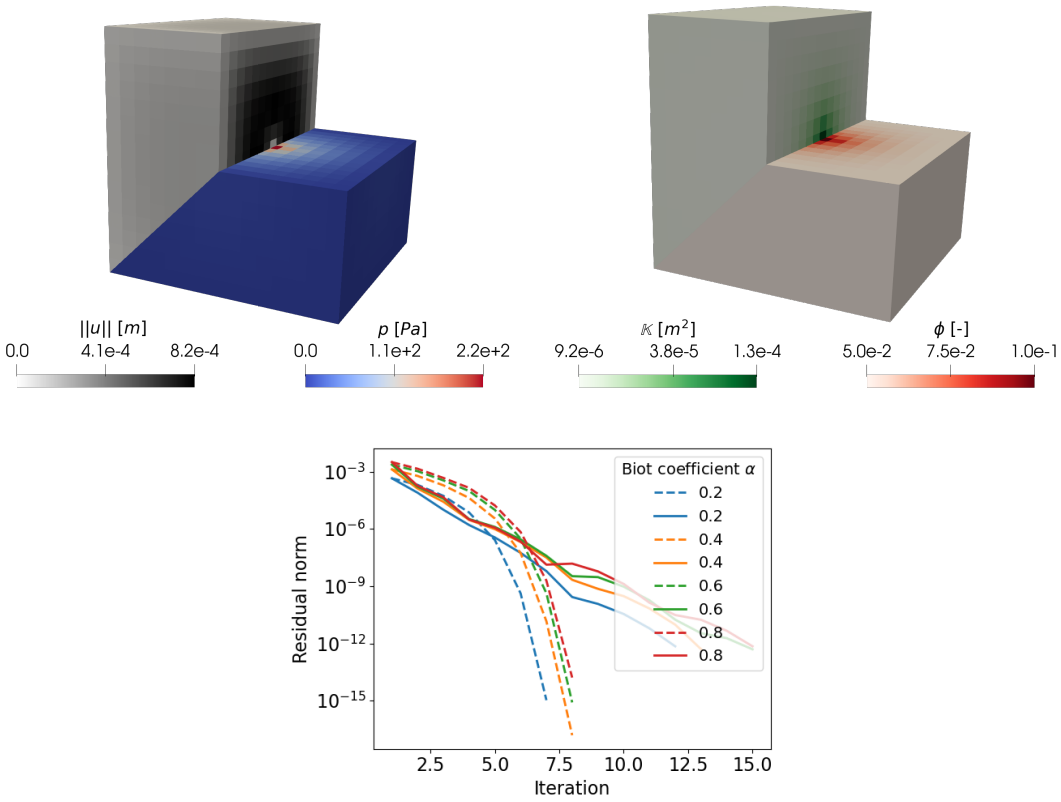

Figure 4. Solution plots for α=0.6 (top) and convergence rates (bottom) for the poroelasticity simulation. We show displacement magnitude ($\|u\|$) and pressure (p) to the left and permeability ($\mathbb{K}$) on a logarithmic scale and porosity (ϕ) to the right.

verges quadratically for all cases and is sensitive to α only in the pre-quadratic regime. In contrast, while competitive in the first iterations, the TP residuals deviate considerably in later iterations and the residual reduction is only linear. We interpret this as the permeability error dominating the residual only at the latter stage. We also note that while TP converges only linearly, the rate is sufficient to achieve convergence in approx. 15 iterations.

4.2.3 Deforming high-permeable fracture

Finally, we expand the poroelastic simulation presented above by including a throughgoing horizontal fracture. The fracture introduces additional nonlinearities through the cubic law dependency of permeability on fracture opening defined in Eq. (12), as well as through the fracture contact mechanics relations of Eq. (17).

The source location is at $(0.5, 0.5, 0.5)$ as above, now corresponding to the center of the fracture. The fracture grid's 225 cells conform to faces in the matrix grid, which consists of 3360 3d cells. As in the poroelastic simulation, fluid injection leads to elevated pressures, and thus alterations of the displacement and permeability fields. The elevated pressure in the fracture leads to significant increases in the fracture aperture.

To control the size of the nonlinear update, we consider a series of simulations with four different injection rates. The residual convergence are shown at the bottom of Fig.

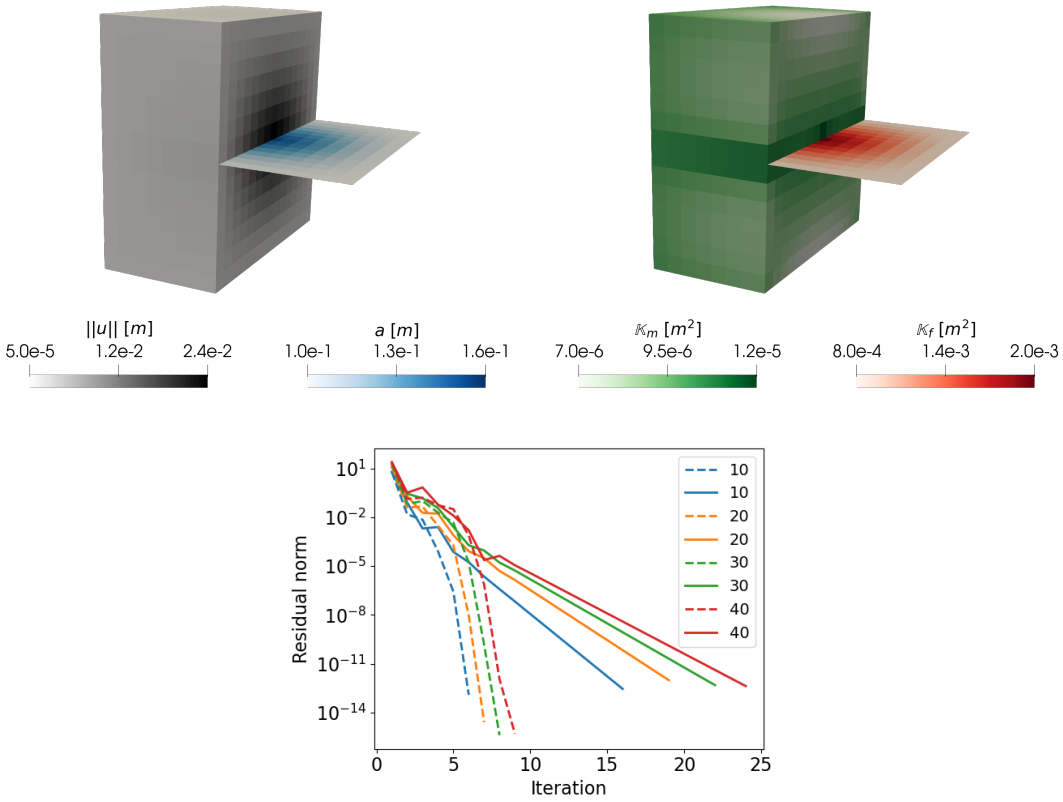

Figure 5. Solution plots for the second highest source rate (top) and convergence rates (bottom) for the deforming fracture simulation. We show matrix displacement magnitude ($\|u\|$) and fracture aperture (a) to the left and permeability in matrix ($\mathbb{K}_m$) and fracture ($\mathbb{K}_f$) to the right. Convergence plot labels correspond to the four source rates in $\mathrm{kg\,s^{-1}}$.

5. The range is chosen such that the fracture cells remain almost in contact ($[u]_n = 0$) for the lowest value and approximately half of the fracture cells are open ($[u]_n > 0$) for the highest one. This corresponds to a transition from an almost constant fracture permeability to a highly variable one.

For the higher source rates, TP convergence rates are decidedly reduced compared to Section 4.2.2 due to the presence of the additional nonlinearities related to the fracture. The differentiated model converges rapidly and quadratically, albeit with some initial iterations with residuals similar to the non-differentiated one. We attribute this to the residual at the initial stage being dominated by nonlinearities other than the permeability. In particular, the contact mechanics cannot in general be expected to converge quadratically.

5 Summary and conclusions

This paper studies the solution of the nonlinear equation system arising in simulations where state-dependent diffusion tensors are discretized by finite volume methods. In contrast to the common approach of ignoring dynamic permeability effects during linearization, we propose a linearization that includes the effect of permeability updates. The added term is derived based on the two-point flux approximation and thereby

easy to implement. Our approach can be applied independent of which finite volume method is used to discretize the diffusion problem: If the original method is also a two-point flux, our method renders an exact linearization. For other discretizations, herein exemplified by a multi-point flux approximation, the linearization is not exact, but its enhanced approximation quality can improve the Newton convergence.

As our illustrative examples, we consider multiphysics problems in which the permeability depends (nonlinearly) on the primary variables. Our simulations illustrate slow convergence if the permeability update is neglected when solving the nonlinear problems. We achieve major improvements when the update is included both for the pure two-point scheme and for the combined scheme.This firstly demonstrates that state-dependent permeability is a major source of nonlinearity in important multiphysics applications. Secondly, it shows the effectiveness of the suggested approach and its potential for speeding up multiphysics simulations. Taken together, this shows that the new approach can be a useful addition to application-oriented simulations of multiphysics problems.

6 Open Research

The data and source code for the results presented herein is available, and the results can be reproduced, using a Docker container available at `https://dx.doi.org/10.5281/zenodo.7624095`.

Acknowledgments

I. Stefansson's work was funded by the VISTA program, The Norwegian Academy of Science and Letters and Equinor. The work of E. Keilegavlen was financed in part by Norwegian Research Council Grant 308733.

References

Aavatsmark, I. (2002). An introduction to multipoint flux approximations for quadrilateral grids. *Computational Geosciences*, *6*, 405-432. doi: 10.1023/A:1021291114475

Anderson, D. G. (1965). Iterative procedures for nonlinear integral equations. *Journal of the ACM (JACM)*, *12*(4), 547–560. doi: 10.1145/321296.321305

Aziz, K., & Settari, A. (1979). *Petroleum reservoir simulation*.

Barton, N., Bandis, S., & Bakhtar, K. (1985). Strength, deformation and conductivity coupling of rock joints. In *International journal of rock mechanics and mining sciences & geomechanics abstracts* (Vol. 22, pp. 121–140). doi: 10.1016/0148-9062(85)93227-9

Berge, R. L., Berre, I., Keilegavlen, E., Nordbotten, J. M., & Wohlmuth, B. (2020). Finite volume discretization for poroelastic media with fractures modeled by contact mechanics. *International Journal for Numerical Methods in Engineering*, *121*(4), 644–663. doi: 10.1002/nme.6238

Bernabé, Y., Mok, U., & Evans, B. (2003). Permeability-porosity relationships in rocks subjected to various evolution processes. *Pure and Applied Geophysics*, *160*(5), 937–960. doi: 10.1007/978-3-0348-8083-1_9

Bollhöfer, M., Schenk, O., Janalik, R., Hamm, S., & Gullapalli, K. (2020). State-of-the-art sparse direct solvers. In *Parallel algorithms in computational science and engineering* (pp. 3–33). Springer. doi: 10.1007/978-3-030-43736-7_1

Both, J. W., Kumar, K., Nordbotten, J. M., & Radu, F. A. (2019). Anderson accelerated fixed-stress splitting schemes for consolidation of unsaturated porous media. *Computers & Mathematics with Applications*, *77*(6), 1479-1502. doi: 10.1016/j.camwa.2018.07.033

Boussinesq, J. (1868). Mémoire sur l'influence des frottements dans les mouvements

réguliers des fluids. *Journal de mathématiques pures et appliquées*, *13*(2), 377–424.

Coussy, O. (2004). *Poromechanics*. John Wiley & Sons.

Dennis Jr, J. E., & Schnabel, R. B. (1996). *Numerical methods for unconstrained optimization and nonlinear equations*. SIAM.

Deuflhard, P. (2005). *Newton methods for nonlinear problems: affine invariance and adaptive algorithms* (Vol. 35). Springer Science & Business Media.

Edwards, M. G., & Rodgers, C. F. (1998). Finite volume discretization with imposed flux continuity for the general tensor pressure equation. *Computational Geosciences*, *2*(259-290). doi: 10.1023/A:1011510505406

Hommel, J., Coltman, E., & Class, H. (2018). Porosity–permeability relations for evolving pore space: a review with a focus on (bio-) geochemically altered porous media. *Transport in Porous Media*, *124*(2), 589–629. doi: 10.1007/s11242-018-1086-2

Hüeber, S., & Wohlmuth, B. I. (2005). A primal–dual active set strategy for nonlinear multibody contact problems. *Computer Methods in Applied Mechanics and Engineering*, *194*(27-29), 3147–3166. doi: 10.1016/j.cma.2004.08.006

Jenny, P., Lee, S. H., & Tchelepi, H. A. (2006). Adaptive fully implicit multi-scale finite-volume method for multi-phase flow and transport in heterogeneous porous media. *Journal of Computational Physics*, *217*(2), 627-641. doi: 10.1016/j.jcp.2006.01.028

Jenny, P., Tchelepi, H. A., & Lee, S. H. (2009). Unconditionally convergent nonlinear solver for hyperbolic conservation laws with s-shaped flux functions. *Journal of Computational Physics*, *228*(20), 7497-7512. doi: 10.1016/j.jcp.2009.06.032

Jiang, J., & Tchelepi, H. A. (2019). Nonlinear acceleration of sequential fully implicit (sfi) method for coupled flow and transport in porous media. *Computer Methods in Applied Mechanics and Engineering*, *352*, 246-275. doi: 10.1016/j.cma.2019.04.030

Keilegavlen, E., Berge, R., Fumagalli, A., Starnoni, M., Stefansson, I., Varela, J., & Berre, I. (2021). Porepy: an open-source software for simulation of multiphysics processes in fractured porous media. *Computational Geosciences*, *25*(1), 243-265. doi: 10.1007/s10596-020-10002-5

Keilegavlen, E., & Nordbotten, J. M. (2017). Finite volume methods for elasticity with weak symmetry. *International Journal for Numerical Methods in Engineering*, *112*(8), 939–962. doi: 10.1002/nme.5538

Krogstad, S., Lie, K. A., Møyner, O., Nilsen, H. M., Raynaud, X., & Skaflestad, B. (2015). Mrst-ad - an open-source framework for rapid prototyping and evaluation of reservoir simulaiton problems. In *Proceedings of the SPE reservoir simulation symposium*.

Li, J., Tomin, P., & Tchelepi, H. (2021). Sequential fully implicit newton method for compositional flow and transport. *Journal of Computational Physics*, *444*. doi: 10.1016/j.jcp.2021.110541

List, F., & Radu, F. A. (2016). A study on iterative methods for solving richards' equation. *Computational Geosciences*, *20*(2), 341-353. doi: 10.1007/s10596-016-9566-3

Martin, V., Jaffré, J., & Roberts, J. E. (2005). Modeling fractures and barriers as interfaces for flow in porous media. *SIAM Journal on Scientific Computing*, *26*(5), 1667-1691. doi: 10.1137/s1064827503429363

Møyner, O. (2017). Nonlinear solver for three-phase transport problems based on approximate trust regions. *Computational Geosciences*, *21*(5), 999–1021. doi: 10.1007/s10596-017-9660-1

Nocedal, J., & Wright, S. J. (1999). *Numerical optimization*. Springer.

Nordbotten, J. M. (2016). Stable cell-centered finite volume discretization for biot equations. *SIAM Journal on Numerical Analysis*, *54*(2), 942–968.

Nordbotten, J. M., Boon, W. M., Fumagalli, A., & Keilegavlen, E. (2019). Unified approach to discretization of flow in fractured porous media. *Computational Geosciences*, *23*(2), 225-237. doi: 10.1007/s10596-018-9778-9

Radu, F. A., Nordbotten, J. M., Pop, I. S., & Kumar, K. (2015). A robust linearization scheme for finite volume based discretizations for simulation of two-phase flow in porous media. *Journal of Computational and Applied Mathematics*, *289*, 134-141. doi: 10.1016/j.cam.2015.02.051

Rasmussen, A. F., Sandve, T. H., Bao, K., Lauser, A., Hove, J., Skaflestad, B., ... Thune, A. (2021). The open porous media flow reservoir simulator. *Computers & Mathematics with Applications*, *81*, 159-185. doi: 10.1016/j.camwa.2020.05.014

Richards, L. A. (1931). Capillary conduction of liquids through porous mediums. *Physics*, *1*(5), 318–333. doi: 10.1063/1.1745010

Schneider, M., Flemisch, B., Helmig, R., Terekhov, K., & Tchelepi, H. (2018). Monotone nonlinear finite-volume method for challenging grids. *Computational Geosciences*, *22*(2), 565-586. doi: 10.1007/s10596-017-9710-8

Shapiro, S. A. (2015). *Fluid-induced seismicity.* Cambridge University Press.

Stefansson, I., Berre, I., & Keilegavlen, E. (2021). A fully coupled numerical model of thermo-hydro-mechanical processes and fracture contact mechanics in porous media. *Computer Methods in Applied Mechanics and Engineering*, *386*, 114122. doi: https://doi.org/10.1016/j.cma.2021.114122

Stefansson, I., & Keilegavlen, E. (2023). *Runscripts for numercial treatment of variable permeability in multiphysics problems.* Retrieved from `https://dx.doi.org/10.5281/zenodo.7624095`

Su, S., Dong, Q., & Wu, J. (2018). A decoupled and positivity-preserving discrete duality finite volume scheme for anisotropic diffusion problems on general polygonal meshes. *Journal of Computational Physics*, *372*, 773–798. doi: 10.1016/j.jcp.2018.06.052

Walker, H. F., & Ni, P. (2011). Anderson acceleration for fixed-point iterations. *SIAM Journal on Numerical Analysis*, *49*(4), 1715–1735. doi: 10.1137/10078356X

Wang, X., & Tchelepi, H. A. (2013). Trust-region based solver for nonlinear transport in heterogeneous porous media. *Journal of Computational Physics*, *253*, 114-137. doi: 10.1016/j.jcp.2013.06.041

Willis-Richards, J., Watanabe, K., & Takahashi, H. (1996). Progress toward a stochastic rock mechanics model of engineered geothermal systems. *Journal of geophysical research: solid earth*, *101*(B8), 17481–17496. doi: 10.1029/96JB00882

Zhou, Y., Tchelepi, H. A., & Mallison, B. T. (2011). Automatic differentiation framework for compositional simulation on unstructured grids with multi-point discretization schemes. In *Proceedings of the SPE reservoir simulation symposium.*